Composite Structures 232 (2020) 111561

Contents lists available at ScienceDirect

Composite Structures

journal homepage: www.elsevier.com/locate/compstruct

Ultra-light release device integrated with screen-printed heaters for CubeSat's deployable solar arrays

Dou Zhang[a], Liwu Liu[a], Jinsong Leng[b,*], Yanju Liu[a,*]

[a] Department of Astronautical Science and Mechanics, Harbin Institute of Technology, Harbin 150001, People's Republic of China
[b] National Key Laboratory of Science and Technology on Advanced Composites in Special Environments, Science Park of Harbin Institute of Technology, Harbin 150080, People's Republic of China

ARTICLE INFO

Keywords:
Shape memory polymer composites
Hold-release mechanism
Screen-printed heaters
CubeSats
Deployable solar arrays

ABSTRACT

Deployable solar arrays can improve the potential utilization of CubeSats by generating sustainable energy. This paper presents an ultra-light release device integrated with screen-printed heaters to latch and release CubeSat's solar arrays in the sequence of structure and material design, fabrication, and experimental verification. Finite element analysis of interference fit gives the locking force and maximum Von Mises stress variation with the interference and thickness, which provides the selection basis for geometrical parameters of the release device. Tensile and fracture toughness tests have been conducted to verify improved toughness for spandex fiber reinforced shape memory polymer composites (SMPCs). And the fine denier fiber shows a better toughness improvement performance. DMA tests have been performed to give the temperature sensitivity of the materials. Besides, locking forces obtained from finite element analysis and experiments show good consistency. Moreover, recovery tests confirm the release device with good shape recovery properties and excellent adaptability to energizing conditions. Finally, experiments on a CubeSat prototype qualify the release device with good feasibility, reliable locking performance and satisfactory reusability. This work is expected to provide an effective miniaturized hold-release mechanism for deployable structures.

1. Introduction

CubeSat has provided extensive space explorations and substantially reduced costs [1,2]. Its power demand has aggrandized continuously with the increasing payloads and more sophisticated functions. Deployable solar arrays therefore appeared because they can potentially generate more electricity [3,4]. They must be stowed during launch and deployed on-orbit appropriately, which needs to be accomplished by hold-release mechanisms (HRMs) [5]. A combination of HRMs and spring-loaded hinges for deployable panels is a simple and reliable solution. Explosive devices, a widely used choice in traditional solar arrays, however are not applicable for their large impact and non-reusable property [6]. Therefore, many efforts have been applied to the study of HRMs with non-explosive actuators.

Adam Thurn et al. proposed a burn wire system composed of a nichrome cutter and Vectran wire [7]. They tested the mechanism in air at room temperature and in vacuum at temperatures of −50 °C and 70 °C. It had cutting times varying from 2.4 s to 7.2 s, and 400 firings without any failure. Subsequently, this burn wire release mechanism was modified by Myeong-Jae Lee et al. to possess higher constraint force and reduced system complexity [8]. Burn wire HRMs have been verified by launch and on-orbit environmental tests and are an experienced non-explosive actuator. The release can also be triggered by shape memory alloys (SMAs). In 2011, a repeatable and resettable spring-type actuator was proposed [9]. It had a release time of 55 s and ultimate preload of 1510 N, and generated a maximum shock lever of −11.09G. Two-year later, this spring-type actuator was successfully verified on board a rocket by measuring and observing the oscillations of the solar panel [10]. Besides, other types of SMA actuators were also designed. In 2013, a wire type SMA actuator was proposed [11]. It had the release time, preload capacity and maximum shock lever of 50 ms, 15 kN and 350 G, respectively. The release time and constraint force have been improved remarkably. Then in 2017, a rotary SMA actuator was designed for a multi-use application [12]. It can be commanded to different angles and thus be used to increase power generation and reconfigure deployable structures. Other release schemes include those employing the principle of different coefficients of thermal expansion [13] and using a combination of torsion spring and micro-lever [14].

Shape memory polymers (SMPs) and their composites (SMPCs) have the property to maintain temporary configurations and recover to their

* Corresponding authors.
E-mail addresses: lengjs@hit.edu.cn (J. Leng), yj_liu@hit.edu.cn (Y. Liu).

https://doi.org/10.1016/j.compstruct.2019.111561
Received 17 April 2019; Received in revised form 18 August 2019; Accepted 9 October 2019
Available online 12 October 2019
0263-8223/

original shapes under the stimuli of thermal, electrical, light and changing magnetic field etc. [15,16]. This shape memory effect brings them high academic value and application prospects in deployable structures and release devices. Compared with SMAs, SMPs have the advantages of low density, large deformation capacity and low cost [15], which will reduce the weight and cost of CubeSats. Temperature sensible SMPs and SMPCs have developed into different kinds of components including hinge [17], truss [18] and antenna [19]. Deployments of these components need to be activated by elevated temperature. This high temperature is usually produced by Joule heating of resistor heaters. For instance, in literature [20], heaters are stuck on the surface of the integrative hinge, of which the maximum strain is 6%. In fact, strains are often smaller than 10% due to the thin shell structure [15]. Stuck on the surface is a valid scheme in these cases. However, the strain in this work is more than 15% due to the larger bending angle, smaller bending radius and thick-walled structure. Resistor heaters thus cannot be stuck on surfaces with the requests of bound together and no break of resistance wire simultaneously. Therefore, screen-printed heaters with the advantages of structural integrity and good flexibility are used [21,22].

The aim of this work is to present an HRM with the non-explosive actuator made of spandex fiber reinforced SMPC. The results are encouraging and show that this HRM has the structural and functional integration, excellent adaptability to energizing conditions and good feasibility on CubeSats. It weighs only 6 g, and the release device (non-explosive actuator) weighs less than 1 g. Tensile and fracture toughness tests have been conducted to explore the toughness improvement of SMPCs. The locking force is simulated and tested with consistent results. Also, shape memory recovery tests have been performed to investigate the shape memory effect and deployable properties. Feasibility study on a 3U CubeSat gives the release device a promising engineering application.

2. Design and fabrication

2.1. Schematic design

A combination of HRM and spring hinge is also used for deployment in Fig. 1. The mechanism is comprised a curved release device and a locking member, of which the former is made of SMPC and connected to the main part of the satellite, and the latter is aluminum and linked with the deployable panel. These two components are both designed to be semi-cylindrical shape with interference to produce the locking force. And the non-explosive actuator (SMPC release device) is studied in detail. This device adopts an initial flat and temporary curved shape of 180° bending angle. The deployment is achieved when SMPC release device recovers to its original flat shape and the deployable panel thus rotates outward 90° under the function of pre-loaded torsion spring. And the envelope size of HRM both in packaged and deployable configurations has been listed in Table. 1. It can be concluded that this HRM is a miniaturized mechanism and can also be adapted to other small spacecrafts.

The release device, which is previously described as the non-explosive actuator, is actuated by temperature. Different from the existing resistor heaters encapsulated by polyimide film, screen-printed heaters are selected for their good flexibility. As shown in Fig. 2(a) with active circuits highlighted in red, we have designed two patterns of serpentine heaters called ‘Type A’ and ‘Type B’, which are parallel and vertical to the length direction, respectively. For each type, two circuits form the redundancy design, and they are denoted by ‘I’ and ‘O’ which means the inner and outer one. The heating reliability is further improved by two heaters printed on each surface of every release device. The heating modes are divided into eight types including two double-circuit and six single-circuit heaters in Fig. 2(b) according to which circuit on each surface is energized (highlighted in red color).

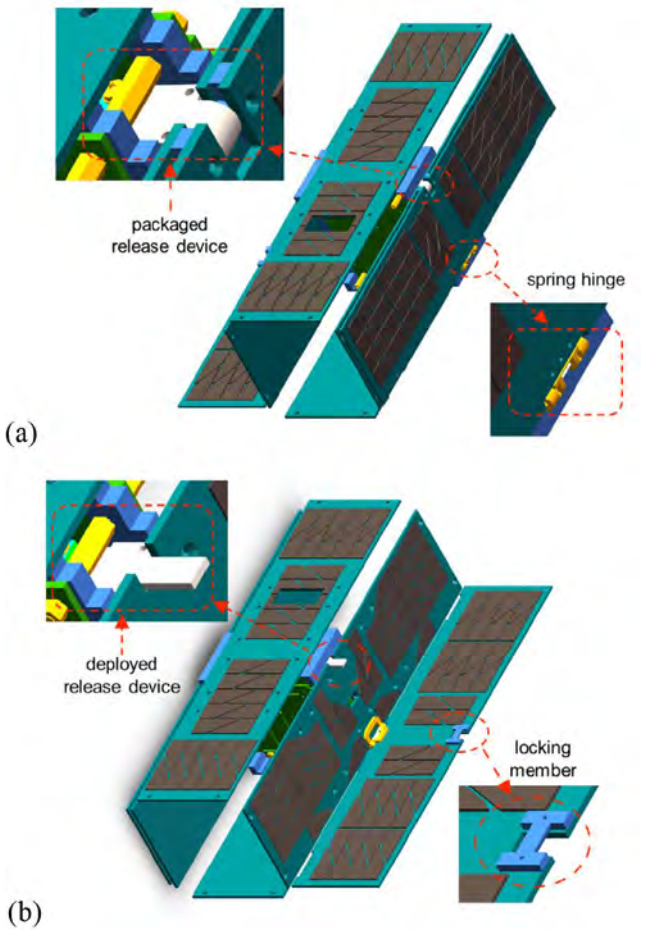

Fig. 1. Schematics of the ultra-light release device. (a) Packaged configuration, (b) deployed configuration.

Table 1
Envelope size of the release device in packaged and deployable configurations.

Characteristic	Packaged configuration	Deployable configuration
Length (mm)	16.6	32
Width (mm)	13	13
Height (mm)	9	1.5
Thickness (mm)	1.5	1.5

2.2. Material design

Epoxy-based SMP [23] has been verified applicable for aerospace and is used in this work. However, the pure SMP easily fracture in the glassy state because of bad conditions in space, such as vibration, shock, changing temperature between high and low. Elastic fibers comprising of 20% spandex and 80% of nylon have been reported to improve the elongation of pure SMP [24]. However, the SMPCs in this reference with 20% and 40% fiber volume fractions show a significant decrease of Young’s modulus and strength, which is unacceptable for the load capacity of HRMs. In order to obtain the small decrease of Young’s modulus and improved toughness at the same time, spandex with superior stretch and elastic recovery properties is used as the reinforcement. According to classical lamination theory, Young’s modulus in the direction of the fibers is given by

$$E = E_m(1 - E_f) + E_f V_f \quad (1)$$

Here, the E_m and E_f are Young’s moduli of matrix and spandex fiber, respectively. V_f represents the fiber volume fraction. And the modulus

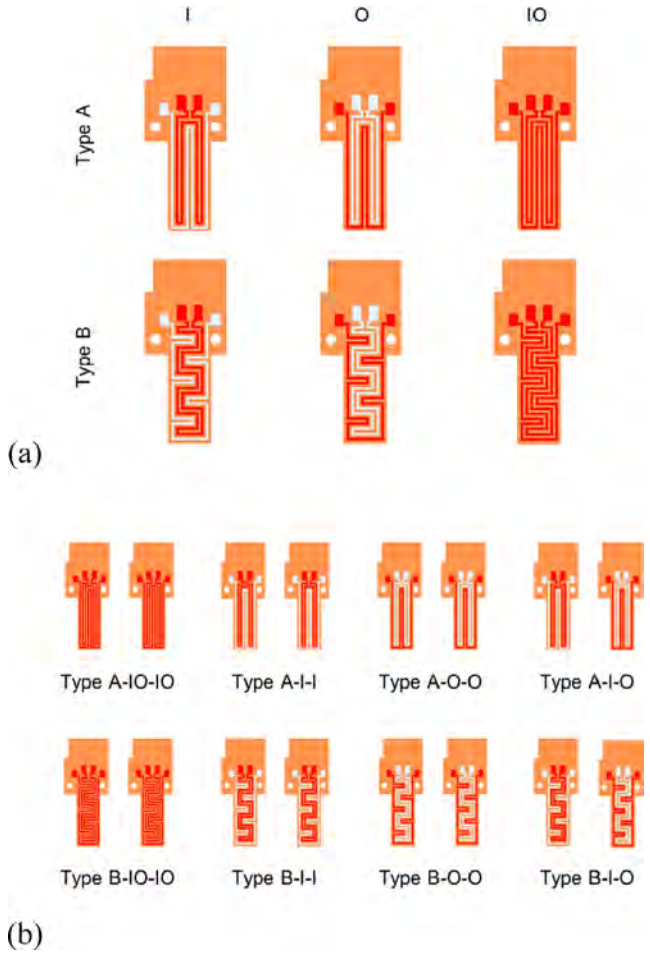

Fig. 2. Layouts of serpentine heaters with active circuits highlighted in red color. (a) Naming methods in detail, (b) eight types of heating mode.

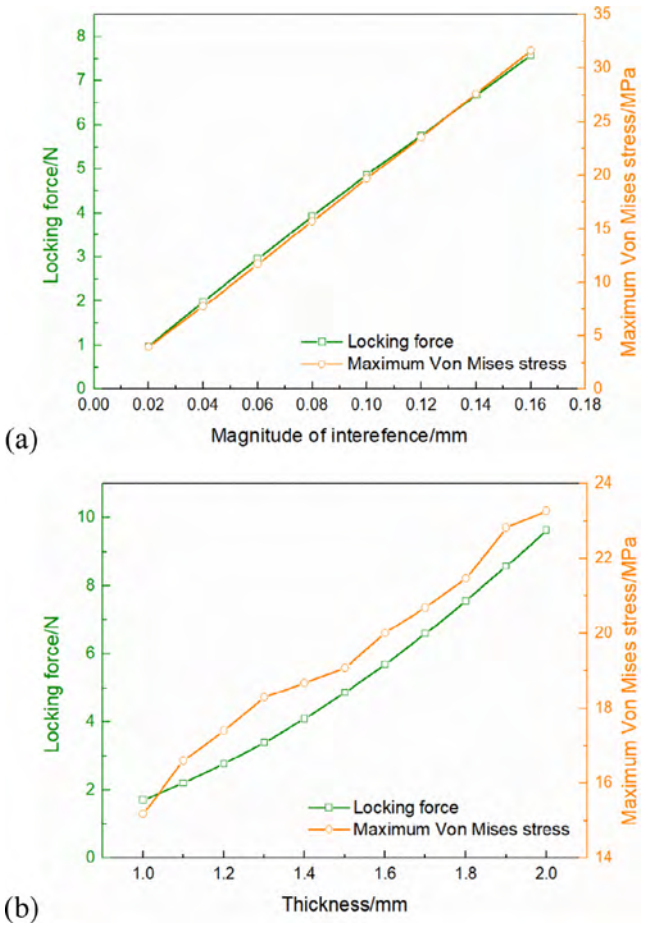

Fig. 3. Locking force and maximum Von Mises stress (a) varying with magnitude of interference, (b) varying with thickness.

of spandex fiber is far less than SMP and can be neglected, the Eq. (1) thus can be simplified as

$$E = E_m(1 - E_f) \tag{2}$$

Pure SMP and SMPCs reinforced by spandex fibers 77.8detx (SMPC-77.8dtex) and 141.4dtex (SMPC-141.4dtex) are selected for analysis. The diameters of these two fibers are 90 μm and 126 μm, respectively, measured by an optical microscope. Fibers are laid for four layers, and one fiber per 0.5 mm and 1 mm, respectively, resulting in a same fiber volume fraction of 3.3%, approximately. Composites with higher fiber content and finer fibers are abandoned due to the lowered Young' modulus and increased difficulty of fabrication, respectively.

2.3. Geometry design

The locking force is one of the most important characteristics of HRMs, and the detailed analysis and geometry design of the release device will be given in this part. Finite element software ABAQUS is used to simulate the assembly of the release device and locking member. The locking force is provided by the release device pre-strained by the locking member with a larger radius. Locking member with an inner radius of 3 mm, release devices with thickness from 1 mm to 2 mm and interference varying from 0 to 0.16 mm are analyzed. For release device, the elastic modulus is obtained from tensile tests and Poisson's ratio is chosen from literature [25]. And the material for locking member is aluminum alloy with elastic modulus of 71 GPa and Poisson's ratio of 0.3. The model is meshed by 'Free' technic and 24,384 ten-node modified quadratic tetrahedron elements C3D10M are formed. And boundary conditions are 'Fixed' of two holes on the release device and displacement of locking member along the axis of the cylinder. Furthermore, the surface to surface contact feature is assigned by specifying locking member's outer surface as the master surface and release device's inner one as the slave surface.

The maximal locking force and minimal Von Mises stress are desired. However, the simulation results in Fig. 3 show that they both increase with the growth of interference and thickness of release device. When the thickness is 1.5 mm, these two values both raise linearly from 1 N to 8 N and 5 MPa to 32 MPa as the interference increases from 0.02 mm to 0.16 mm. And when the interference is 0.1 mm, the force and maximum Von Mises stress increase from 1.7 N to 9.6 N and 15 MPa to 23 MPa with the thickness from 1 mm to 2 mm. A compromise between the locking force and Von Mises stress thus needs to be made. This is determined by the material properties of SMPC because it is set to be a liner elastic material in the simulation and according to the tensile tests, the yield strength is 46 MPa approximately. In order to provide a safety margin greater than 1, the release device with interference of 0.1 mm and thickness of 1.5 mm is selected for fabrication and further analysis. Using parameters including thickness of 1.5 mm, bending angle of 180° and bending radius of 2.9 mm (interference of 0.1 mm), the strain of the release device is calculated to be 20.5%. This result validates the decision of abandoning resistor heaters and selecting screen-printed heaters.

The more detailed distribution of Von Mises stress is shown in Fig. 4. The maximum Von Mises stress which is 19.69 MPa appears at the left hole. Stress variation in axial direction (path EBCD) is expressed in Fig. 4(c). Maximum Von Mises stress around 7.4 MPa emerges in the central part of the inner wall (E-B), but the stress gradually decreases to

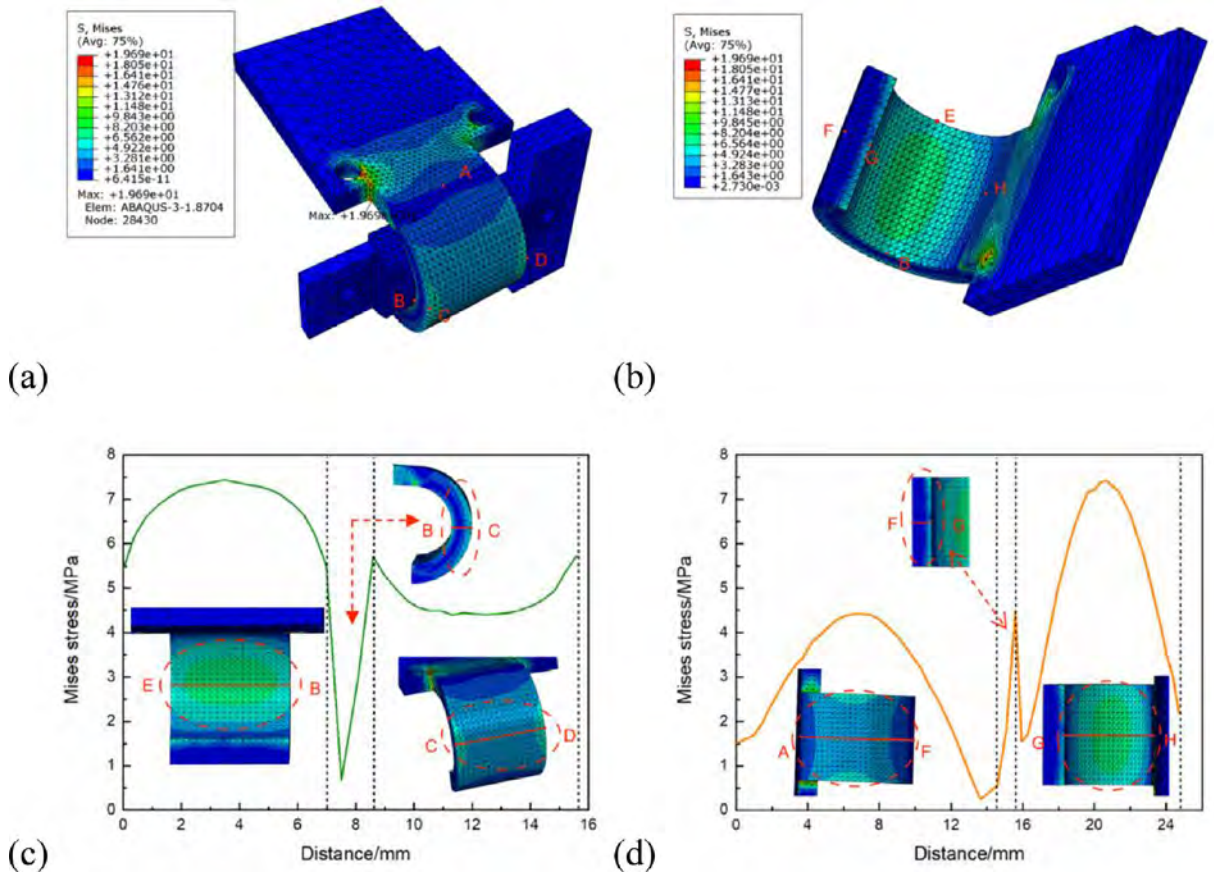

Fig. 4. Von Mises stress distributions from ABAQUS with interference of 0.1 mm and device's thickness of 1.5 mm. (a) external surface, (b) internal surface, (c) along the path EBCD, (d) along the path AFGH.

5.5 MPa on both sides. Besides, stress in radial direction (B-C) is not monotonically decreasing, but first reduces to about 0.6 MPa and then increases to 5.5 MPa. Moreover, the distribution of the outer wall (C-D) is just opposite to that of the inner wall with a minimum of about 4.5 MPa in the middle area. Circumferential results (path AFGH) in Fig. 4(d) always show a larger stress in the center, both in outer (A-F) and inner walls (G-H). Another difference from the axial direction lies in radial distribution (H-G), which is monotonically increasing.

2.4. Fabrication

The resin infusion method is used for fabrication. The procedure in Fig. 5 is same as the literature [17]. Spandex fiber is stacked on a glass plate for four layers manually. The mixed solution of resin, curing agent and modifier is injected into the semi-closed mold formed by two glass plates and rubber strip. The filled mold is then placed in an oven with curing process of three steps: 80 °C for 3 h, 100 °C for 3 h and 150 °C for 5 h and the heating rate is 1 °C/min approximately. The initial flat release device is obtained by a laser cutter with the power of 60% and feed velocity of 10 mm/s. And the heater made of silver conductive ink is printed on this flat sample as shown in Fig. 5 step V. The ink is scraped from the mesh of the printing pattern to SMPC substrate during the movement of squeegee and form a circuit. The steps above are repeated to print another heater on the other surface. Then, the SMPC release device with printed heaters is placed into an oven with temperature of 100 °C for 1 h to cure. Finally, the wire is fixed by polyimide tape and insulation is completed by a thin layer of silicone rubber. The curved shape of release devices is formed as in Fig. 5 step IX. Firstly, the flat release device and inner mold are placed in a 100 °C oven for 10 min. Then, the outer mold is used to bend the soft SMPC. Next, the release device is cooled to room temperature maintaining these two molds. Finally, remove the molds and the curved release device is obtained. This release device with heaters and 400 mm long wires is less than 1 g and the whole HRM is 6 g. Optical micrographs in Fig. 6 show that the line width and separation between two lines are both 0.4 mm and the thickness is 12 μm on average. The resistances of eight types heaters written as 'Type A-IO-IO', 'Type B-IO-IO', 'Type A-I-I', 'Type B-I-I', 'Type A-O-O', 'Type B-O-O', 'Type A-I-O' and 'Type B-I-O' in accordance with Fig. 2(b) are 4.7 Ω, 4.6 Ω, 9.3 Ω, 9.5 Ω, 9.6 Ω, 9.4 Ω, 9.5 Ω, 9.4 Ω, respectively.

3. Experiments

3.1. Mechanical tests for SMP and SMPC plate specimens

3.1.1. Tensile tests

Tensile tests were conducted on a Zwick 050 machine with 5kN load cell in room temperature for a better understanding of material used in ultra-light release device, from which the mechanical properties including the elastic modulus, elongation at break and toughness determined by the area under the stress-strain curves were obtained. Dumbbell specimens for tensile tests were cut according to the standard ASTM-D638 type V. Tensile tests were carried out at a rate of 2 mm/min until broke and the tensile force, displacement and strain were recorded.

3.1.2. Fracture toughness tests

To investigate the toughness improvement by adding spandex fibers and whether the size of fiber influence the fracture, facture toughness tests were managed in accordance with the standard for single-notch three-point bending tests in ASTM-D5045-99. The fracture toughness K_{IC} and fracture energy G_{IC} were obtained from these tests. The

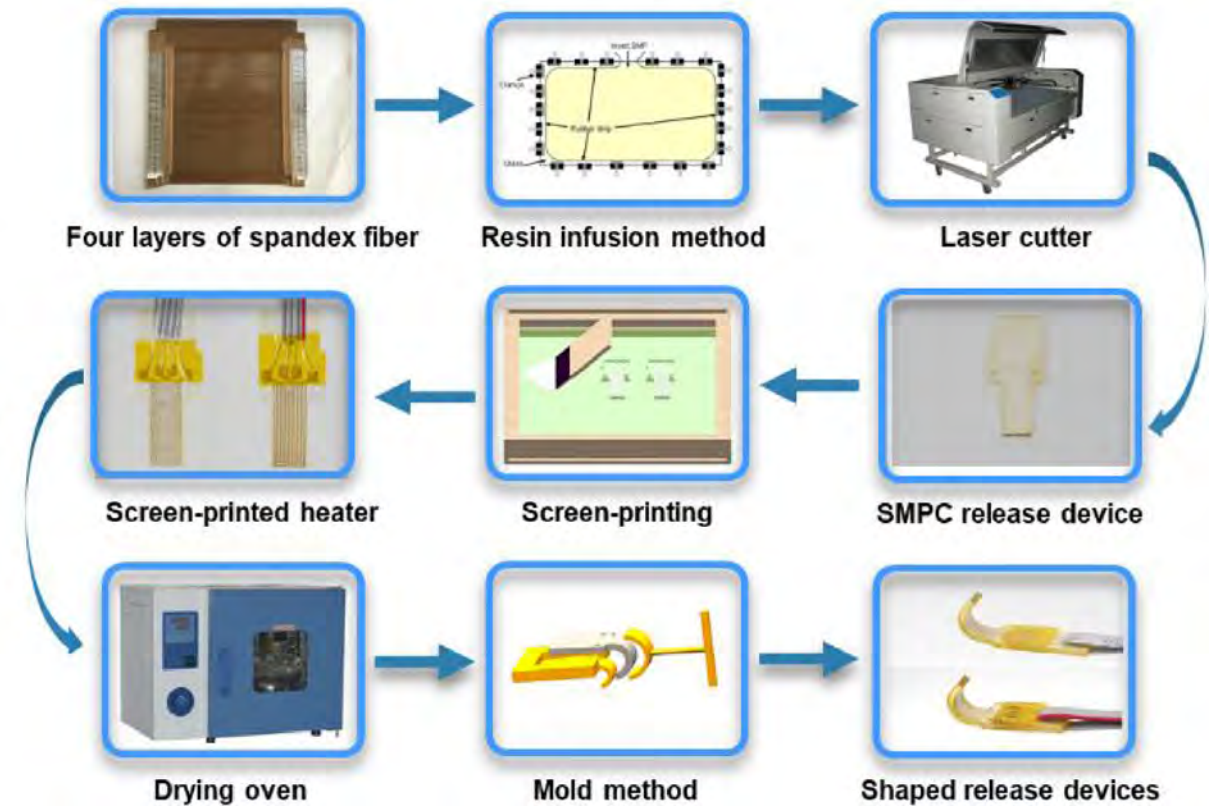

Fig. 5. Schematic of the ultra-light release device fabrication process.

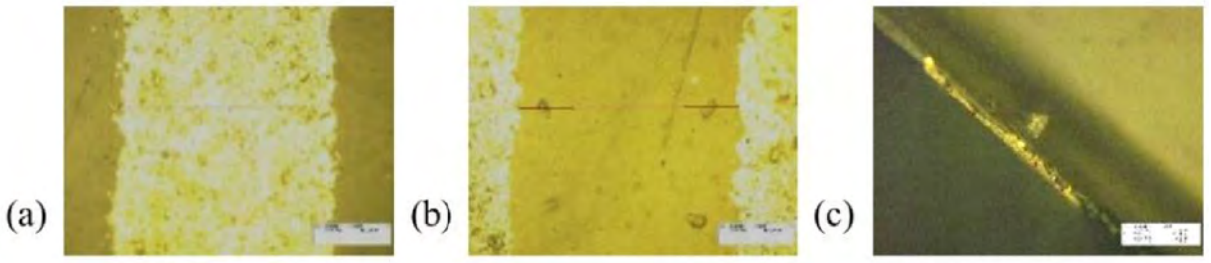

Fig. 6. Optical micrographs. (a) Line width, (b) separation, (c) thickness.

prefabricated opening of specimens was cut by a laser cutter and positioned in the central of the length. The depth of the opening was 0.45 times the width of the specimen. Specimens with a width of 12.7 mm, length of 50.8 mm and support span of 25.4 mm were adopted to perform three-point bending tests. The loading method was constant speed loading of 1 mm/min and the crack was aligned with the pressure head of the test machine. The tests stopped when the deflection of the central point of the span reached 7 mm, and the force and deflection were recorded during the bending process. Fracture morphologies of SMP and SMPCs were observed by an optical microscope.

3.1.3. Dynamic mechanical analysis

The thermo-mechanical properties of SMP and SMPC plays a significant role in the locking and recovery performance of the release device. In order to conduct this dynamic mechanical analysis (DMA), a DMA analyzer (NETZSCH Instruments, Germany) was adopted. Specimens with dimensions of $30 \times 5 \times 1.5\,mm^3$ were tested at a tension oscillatory temperature from 25 °C to 160 °C and at a heating rate of 3 °C/min and frequency of 2 Hz. This analysis would provide us with the variation of the storage modulus and loss factor with temperature. The glass transition temperature (*Tg*) would also be given as the temperature corresponding to the peak value of loss factor. And it was a critical parameter for screen-printed heaters to actuate the shape memory recovery.

3.2. Tests of locking force

Locking properties as one of the most important features of HRMs were tested and the results were used to validate the reliability of finite element analysis. However, due to the restriction of miniaturized structure, the interference fit was simplified into a relative motion of the release device and locking member along the radial direction. This motion was carried out on a tensile machine with an accuracy to three decimal places to improve the precision as much as possible. The setup was shown in Fig. 7 which composed of a release device and fixture with the same radius. The fixture was adjusted to be concentric with the curved release device before testing. And the relative motion was conducted in a tensile mode at a rate of 0.1 mm/min for 1.6 min with the release device fixed. The displacement of the fixture was regarded as the magnitude of interference, and the tensile force served as the locking force.

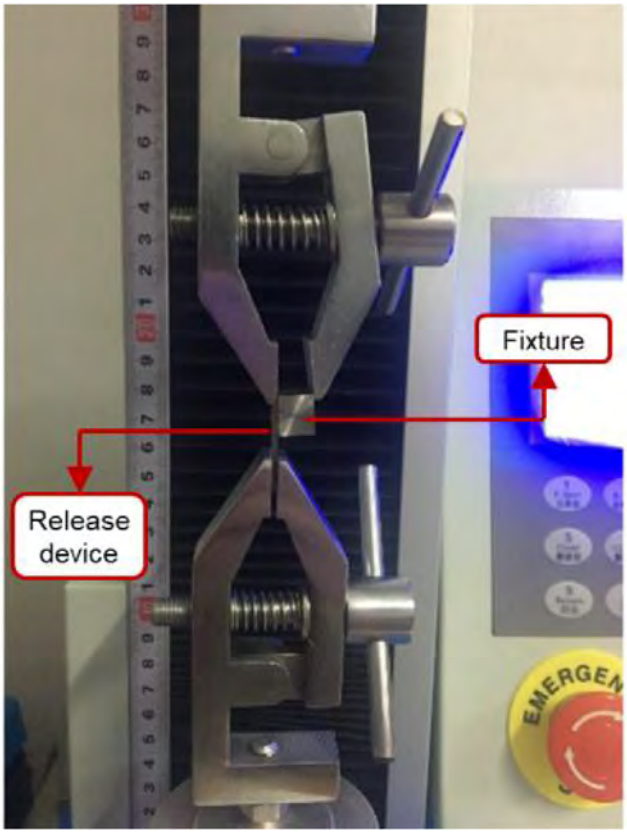

Fig. 7. Setup for tests of locking force.

3.3. Shape memory recovery tests

In order to stimulate the shape memory recovery process, flexible heaters were printed on the surfaces of the release device. Release devices with eight types of heaters as shown in Fig. 2(b) were all subjected to 3 V voltage to investigate their heating performance. Temperatures of two points (point A and point B in Fig. 8) on bending center of each surface were monitored by Hioki MEMORY HiLOGGER LR8400 portable data logger with a recording interval of 100 ms. The free recovery of the release device was monitored by a camera to record the recovery trajectory and a thermal infrared imager (Jenoptik InfraTec, Dresden, Germany) to record the heat field distribution. The shapes and angles measured by camera during the recovery were referred as S_r and θ_r, and the original ones were denoted by S_0 and θ_0 in Fig. 8. The shape

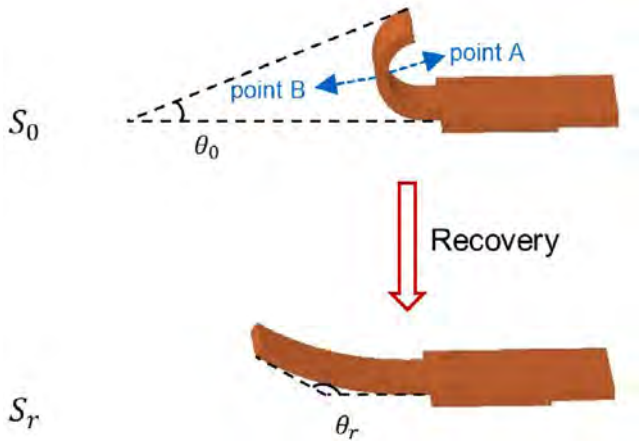

Fig. 8. Calculating method of the recovery ratio.

recovery ratio (R_r) quantifying the shape memory effect was calculated as follows:

$$R_r = \frac{\theta_r - \theta_0}{180^\circ - \theta_0} \times 100\% \quad (3)$$

3.4. Feasibility study on a CubeSat prototype

To investigate the feasibility of this ultra-light release device on CubeSats, experiments including release, thermal cycles and vibration were done with a 3U prototype in Fig. 9. The deployable panel was latched by the curved release device, and the packaged configuration was obtained. For deployable configuration, the release device was heated by the screen-printed heaters with 3V DC voltage, recovering to its original flat state, and the panel was deployed. Reusability is another characteristic which makes SMPC release device superior to explosive actuators and burn wire non-explosive actuators. These tests were conducted by repeating the molding and release process, during which the release times were obtained and morphologies of the release device were observed.

Since the temperature was used as the mechanism to release the deployable panel, premature deployment must be avoided. However, unwanted heating and cooling were inevitable for spacecraft during the storage, launch and flight stages. Therefore, thermal cycling tests were used to simulate this temperature variation process. It consisted of 4.5 cycles and was performed in a Zwick temperature chamber with a temperature variation from −25 °C to 55 °C and changing rate of 3 °C/min in Fig. 9 (b). The tested release device was printed with the heater named 'Type B-IO-IO'. It is significant to find a way to verify the locking property after these thermal cycles for two reasons. On the one hand, as mentioned before, the drastic change in temperature might cause crack propagation and fracture of the SMPC. On the other, the viscoelastic property of SMPC makes the creep more obvious at high temperatures, thus the interference will be diminished as well as the locking force. Therefore, to justify whether the deployable panel could be latched reliably by the release device after thermal cycles, vibration tests were conducted on an electro-dynamic vibration system. Besides, vibration tests were conducted for another reason. The deployable solar arrays render the spacecraft with increased functionality and sustainable energy during the flight. However, these structures are flexible and need to be latched by HRMs to raise their vibration frequency during the launch process. Thus, the mechanical properties of the release device are critical in the vibration. It needs to provide enough locking force to maintain the packaged configuration. Therefore, to investigate whether the CubeSat packaged by the release device after thermal cycles could withstand this harsh mechanical environment, sinusoidal and random vibration tests were conducted. The test conditions were shown in Fig. 9(c) where the red lines represented the upper and bottom limitations and black lines characterized actual plot recorded by the acceleration sensor on the vibration table. Due to the miniaturization of the release device, no data was collected. The results were evaluated by test phenomenon, morphology and release time.

4. Results and discussion

4.1. Mechanical properties of the SMP and SMPC

4.1.1. Static mechanical properties

The curves of the stress versus strain from tensile tests of SMP and SMPC-77.8dtex and SMPC-141.4dtex have been shown in Fig. 10. As predicted by the classical lamination theory, the elastic modulus is decreased from 980 MPa for pure SMP to 945 MPa for SMPC-77.8dtex and 934 MPa for SMPC-141.4dtex. The elongation has been increased from 17.92% for pure SMP to 24.86% for SMPC-77.8dtex and 21.38% for SMPC-141.4dtex. Toughness calculated by the area under the stress-strain curves is 6.64 MJ/m^{-3} for pure SMP, 8.81 MJ/m^{-3} for SMPC-

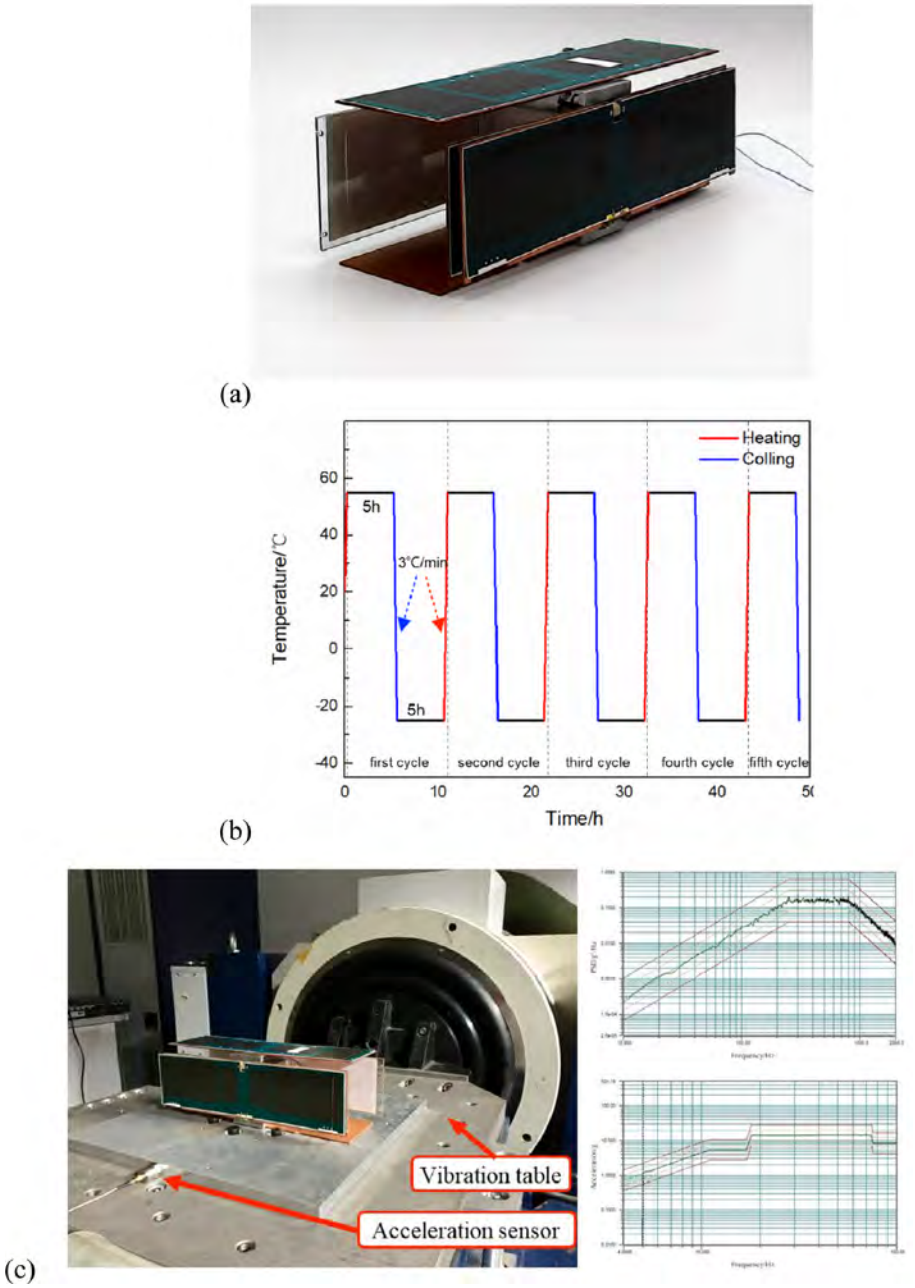

Fig. 9. Tests on a 3U CubeSat prototype. (a) Release tests of solar arrays, (b) temperature curves of thermal cycling tests, (c) setup and control curves of vibration tests.

77.8dtex and 7.61 MJ/m^{-3} SMPC-141.4dtex. SMPC-77.8dtex and SMPC-141.4dtex shows a similar elastic modulus because they have the same fiber volume fraction. And this decrease compared with modulus of SMP is neglectable and acceptable. Whereas the elongation of SMPC-77.8dtex is greater than that of SMPC-141.4dtex, and the toughness of SMPC-77.8dtex is also greater.

The fracture process of spandex fiber reinforced SMPCs can be divided into two stages named crack formation and crack propagation. The crack can be formed in the process of curing or laser cutting. It comes from the microscopic defect inside the material. When the material is subjected to mechanical or thermal load, the crack tip stress will increase. And when the stress reaches to a certain value, the crack will expand forward. During crack propagation, the crack tip may encounter various damages, which accelerate the crack growth and eventually break the material. Mode I facture toughness K_{IC} is the critical value of the stress intensity factor and it is determined by the following equations:

$$K_{IC} = \frac{P_Q}{BW^{\frac{1}{2}}} f\left(\frac{a}{W}\right) \tag{4}$$

where the $f\left(\frac{a}{W}\right)$ is the shape factor and is calculated by:

$$f\left(\frac{a}{W}\right) = \frac{6\left(\frac{a}{W}\right)^{\frac{1}{2}}\left[1.99 - \frac{a}{W}\left(1 - \frac{a}{W}\right)\left(2.15 - 3.93\frac{a}{W} + \frac{2.7a^2}{W^2}\right)\right]}{\left(1 + \frac{2a}{W}\right)\left(1 - \frac{a}{W}\right)^{\frac{3}{2}}} \tag{5}$$

$$B,\ a,\ W - a \geq 2.5\left(\frac{K_Q}{\sigma_{YS}}\right)^2 \tag{6}$$

Here P_Q is the critical load, and from Fig. 11, for SMP, SMPC-77.8dtex and SMPC-141.4dtex, it is 28.45 N, 32.55 N and 31.11 N, respectively. B, W and a are thickness, width of specimens and length of

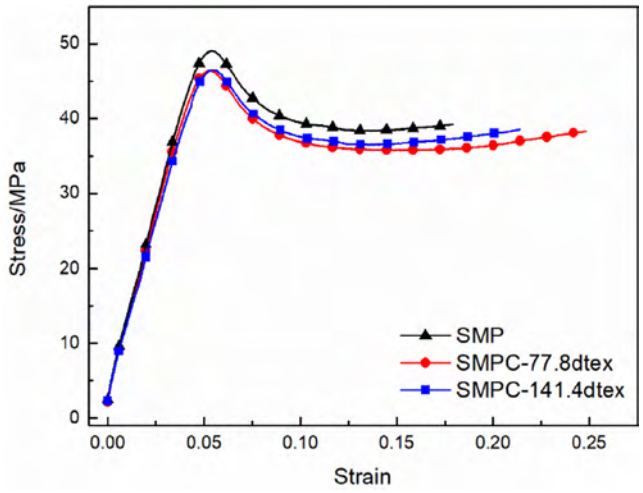

Fig. 10. Experimental curves of stress versus strain from tensile tests.

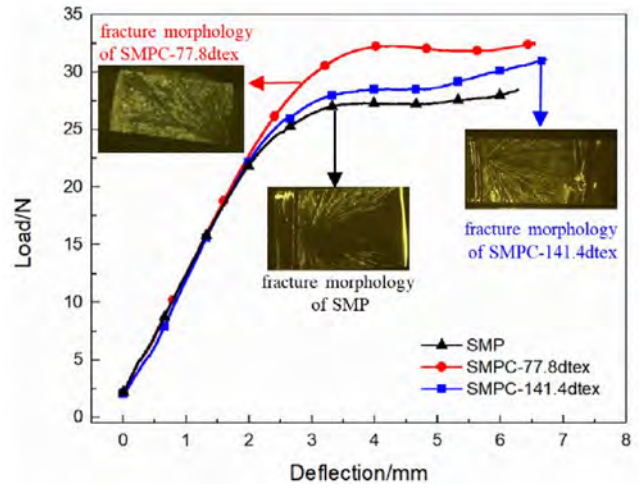

Fig. 11. Experimental curves of load versus deflection from fracture toughness tests.

preformed crack. σ_{YS} is the yield strength and from tensile tests, it is 49.01 MPa, 46.25 MPa and 46.43 MPa for SMP, SMPC-77.8dtex and SMPC-141.4dtex. Eq. (6) is satisfied for the dimensions of the tested specimens.

The crack propagation is initiated when the energy release rate reaches its critical value G_{IC}. It is the energy per unit area lost as the material fractures and can be given as:

$$G_{IC} = \frac{(1-\mu^2)K_{IC}^2}{E} \tag{7}$$

where E is the elastic modulus, μ refers to the Poisson's ratio.

The fracture toughness K_{IC} is increased from 1.54 MPa·m$^{1/2}$ for pure SMP to 1.76 MPa·m$^{1/2}$ for SMPC-77.8dtex and 1.68 MPa·m$^{1/2}$ for SMPC-141.4dtex. And fracture energy G_{IC} has been increased from 2123 J·m^{-2} for pure SMP to 2876 J·m^{-2} for SMPC-77.8dtex and 2651 J·m^{-2} for SMPC-141.4dtex. The fracture morphologies in Fig. 11 show that addition of spandex fiber causes many microcracks in composites when they fracture. When cracks propagate to the vicinity of fiber, they continue to expand. Thus, the fracture energy increases, which slows down the damage of the material. Moreover, the fracture morphology of SMPC-77.8dtex shows more microcracks than SMPC-141.4dtex with the same fiber volume fraction. It can be explained that SMPC-77.8dtex has more contacts of fiber and matrix, and when the material suffers external load, the initial cracks have more propagation paths, thus increase the energy release rate and G_{IC} is also increased. The mechanical properties summarized in Table. 2 illustrate that the spandex fiber reinforced SMPCs have the increased elongation at break, toughness, fracture toughness and fracture energy. Compared with SMPC-141.4dtex, SMPC-77.8dtex shows a better improvement performance under the similar reduction in elastic modulus and strength. Therefore, SMPC-77.8dtex is selected for fabrication of the release device and analyzed in the following part.

4.1.2. Thermo-dynamic mechanical properties

The results of dynamic mechanical analysis show the storage modulus and loss factor tan(delta) of pure SMP and SMPC-77.8dtex as a function of temperature in Fig. 12. Tan(delta) is the ratio of loss modulus to storage modulus, the temperature corresponding to the peak value of which is regarded as *Tg*. For SMP and SMPC-77.8dtex, they are 94 °C and 88 °C, respectively. This suggests that the *Tg* is lowered slightly by addition of spandex fibers. The two storage moduli both sharply decrease within the transition region and maintain at a low level above 90 °C. This means two different states named glassy state and rubbery state of the materials. Besides, it can be observed that the storage modulus of SMPC-77.8dtex is smaller than that of SMP, consistent with the results from classical lamination theory.

4.2. Locking properties of the release device

Comparisons of locking force obtained from simulation and experiments for variable interference are illustrated in Fig. 13. Data from simulation is demonstrated in green line, while this from experiments is shown in black line. The experimental results show good consistency with simulated ones, which confirms the feasibility of the simulation method. The maximum relative error between experimental and simulation results is about 16%, which is inevitable and acceptable for such miniaturized structure.

The temperature effect on locking properties is investigated by thermal cycling tests without looseness or fracture observed. Thereafter, vibration tests show no abnormal occurrence for packaged CubeSat latched by the release device. These results confirm the mechanical properties of the packaged CubeSat as well as the locking properties of the release device after thermal cycles. It suggests that this ± 55 °C high-low temperature does not cause fatal creep or fracture of the release device, and the device still shows a reliable locking performance in this harsh mechanical environment. Finally, the deployment of solar panel with a release time of 26 s for 'Type B-IO-IO' under 3V voltage in room temperature proves that the device has a

Table 2
Mechanical properties for SMP and SMPCs plate specimens.

Characterization	SMP	SMPC-77.8dtex	Increment	SMPC-141.4dtex	Increment
Tensile modulus (MPa)	980	945	−3.57%	934	−4.69%
Yield strength (MPa)	49.01	46.25	−5.63%	46.43	−5.26%
Elongation at break (%)	17.92	24.86	38.73%	21.38	19.31%
Toughness (MJ·m^{-3})	6.64	8.81	32.68%	7.61	14.61%
Fracture toughness K_{IC} (MPa·m$^{1/2}$)	1.54	1.76	14.29%	1.68	9.09%
Fracture energy G_{IC} (J·m^{-2})	2123	2876	35.47%	2651	24.87%

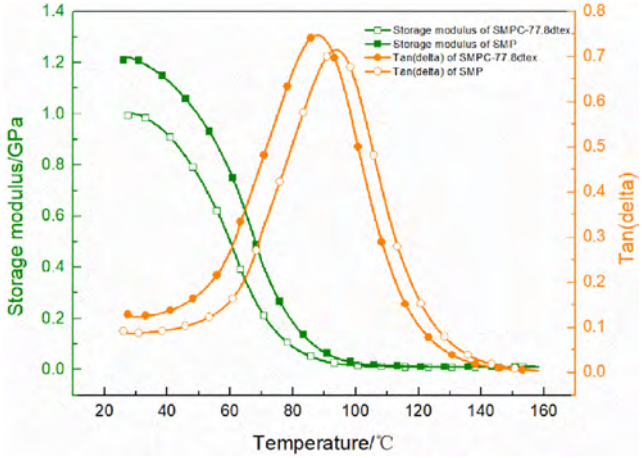

Fig. 12. Experimental curves of storage modulus and tan(delta) versus temperature from DMA.

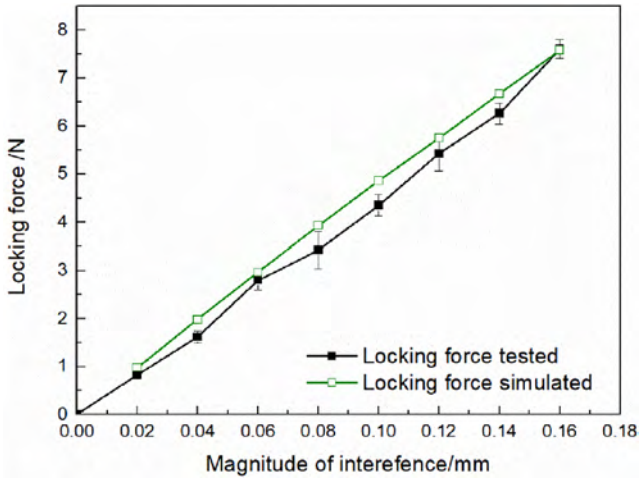

Fig. 13. Curves of locking force versus interference from experiments and simulation.

stable release property. Although there was no direct vibration response, the observations still suggest that the ultra-light release device has a good mechanical resistance, no mechanical or electrical damage occur after thermal cycling and vibration tests. These results imply that neither premature deployment nor damage brought by creep will happen during the launch stage. This is a critical characteristic for components made of temperature sensible shape memory materials.

4.3. Shape memory recovery performance

4.3.1. Shape memory recovery properties of SMPC release device

Shape memory recovery of the release device is triggered by the energized screen-printed heaters. Fig. 14 shows the curves of temperature versus time of eight types of heating modes corresponding to Fig. 2(b). This data is the mean value of temperatures monitored from point A and point B in Fig. 8. These curves begin with a rapid growth in the first 80 s followed by a slowly increase from 80 s to 180 s. The results suggest that the screen-printed heaters powered by 3V voltage produce steady-state temperatures of 140 °C for double-circuit and 100 °C for single-circuit heaters approximately. These temperatures are higher than the glass transition temperature of SMPC-77.8dtex, which indicates that they can actuate the shape memory recovery. A negligible difference is found among the six single-circuit heaters. Therefore, Type A-I-I and Type B-I-I will be analyzed on behalf of the last four types single-circuit heaters in the following part.

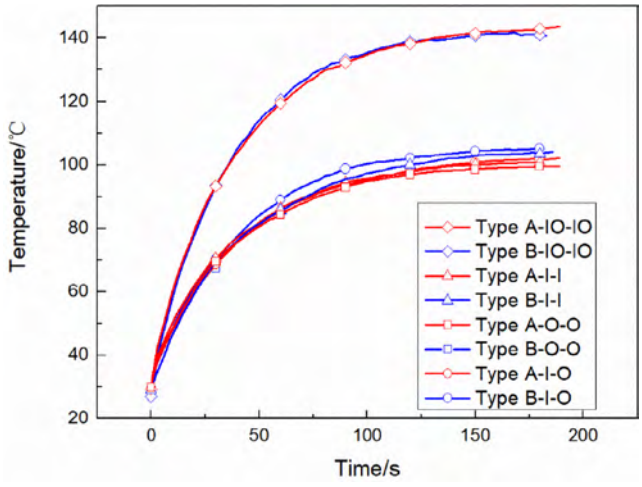

Fig. 14. Curves of temperature versus time under 3V DC voltage.

Fig. 15 shows the detailed recovery process of the release device actuated by first four types of heaters subjected to 3V voltage. The recovery and thermal images suggest that when the ultra-light release device is heated up to a specific starting temperature, there will be a sharp response followed by a slowed recovery to the end. The release devices powered by double-circuit heaters in Fig. 15(a) and (b) show starting time of 25 s, recovery time of 50 s and recovery ratio more than 98%, approximately. Those with single-circuit heaters in Fig. 15(c) and (d) show prolonged starting time of 40 s, recovery time of 65 s and recovery ratio 95%, approximately. These findings suggest that the release device stimulated by single-circuit heaters still has a good shape memory recovery behavior, therefore the heating reliability is increased.

4.3.2. Release of the solar arrays

The release of solar arrays is illustrated by 'Type B-IO-IO' with 3V voltage in Fig. 16. The panel begins to expand at 18 s, and is released and fully deploys in 24 s. The release time of 24 s decreases significantly compared with the free recovery of 47 s. The shape recovery ratio is 61.54% when the deployment is completed, which is obviously lower than free recovery ratio of 99.3%. The shape recovery ratio is thus of little value to judge the deployment, but the release time really matters. Therefore, four types of devices are applied to release solar arrays with the release time recorded. The results show that for release devices with double-circuit and single-circuit heaters, the release times are about 25 s and 40 s, respectively. Compared with free recovery in Fig. 15, these release times show a 50% decline approximately. These changes are mainly caused by SMPC's variable stiffness properties with temperature. The modulus drops dramatically in high temperature and the release is accelerated by external force brought by spring-loaded hinge.

4.3.3. Properties of reusability

Fig. 17 shows the reusability of the release device tested by four types of heaters subjected to 3V voltage. The release times maintain stable with slight fluctuations within 20 cycles of the shape memory process. It is about 25 s for double-circuit heaters and around 40 s for single-circuit heaters. These shape memory cycles create no significant deterioration on the release time. While the morphologies in Fig. 17(b) show some changes. The release device turns yellow after the 20 cycles and it may cause a decline in mechanical properties. Although the reusability of 20 cycles is lower than HRMs made of SMAs, 20 times are enough for ground experiments and orbital application. And it is more reliable and energy-saving than burn wire systems, of which the wire needs to be replaced after every release. Moreover, the ultra-light property and structural integrity is superior than those of SMAs.

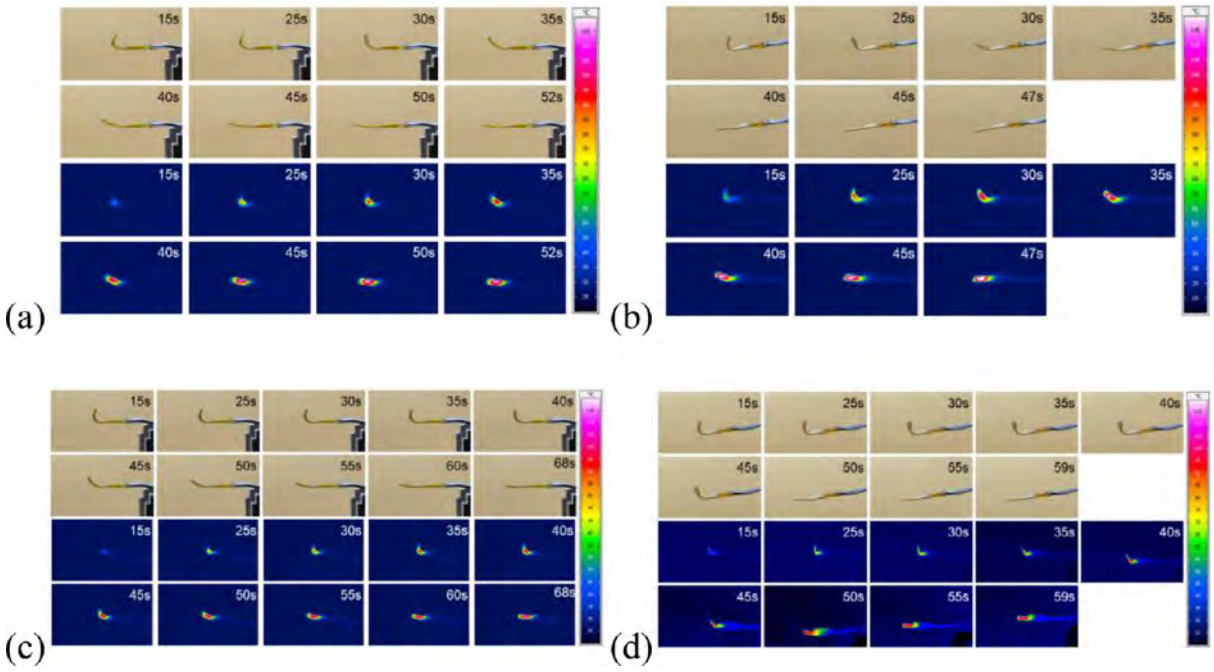

Fig. 15. Images of deployment recorded by both camera and thermal infrared imager under applied 3V DC. (a) Type A-IO-IO, (b) Type B-IO-IO, (c) Type A-I-I, (d) Type B-I-I.

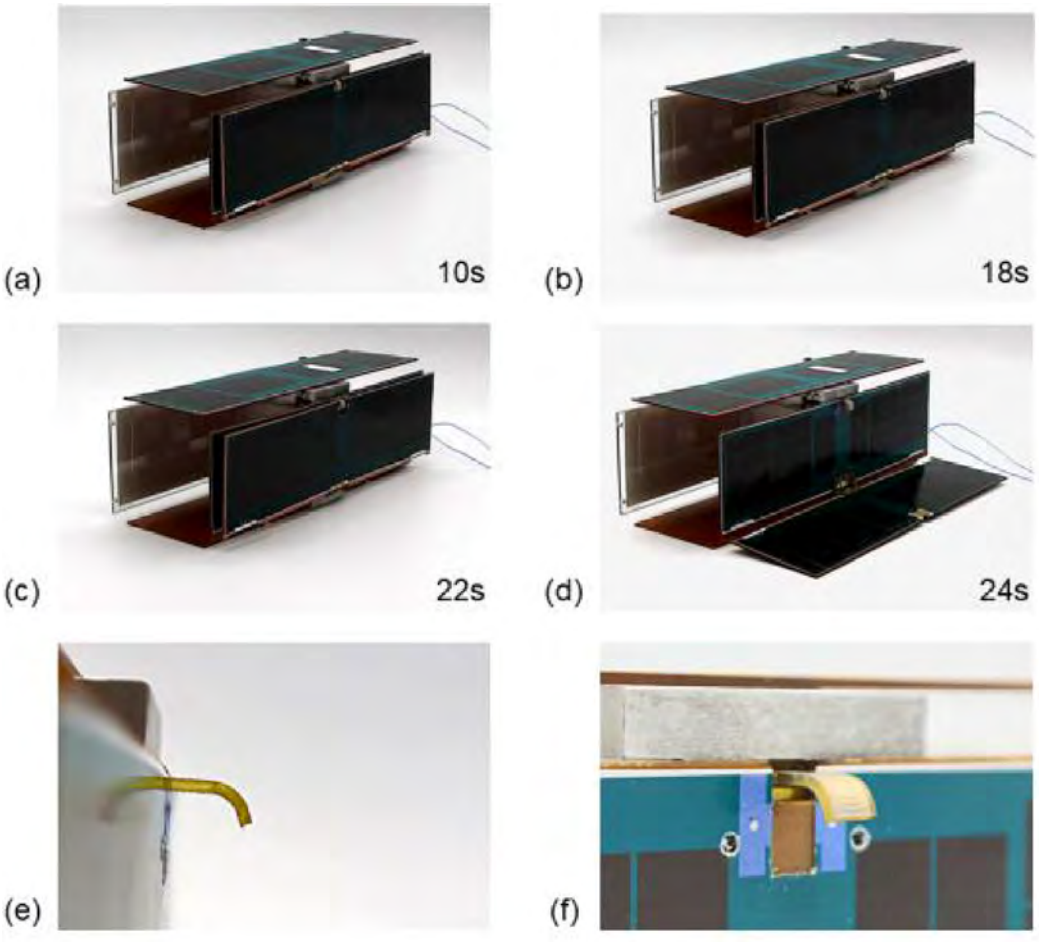

Fig. 16. Deployment of Type B-IO-IO with a 3U CubeSat under applied 3V DC. (a)–(d) Deployment of the solar panel, (e) and (f) ultra-light release device completing release function.

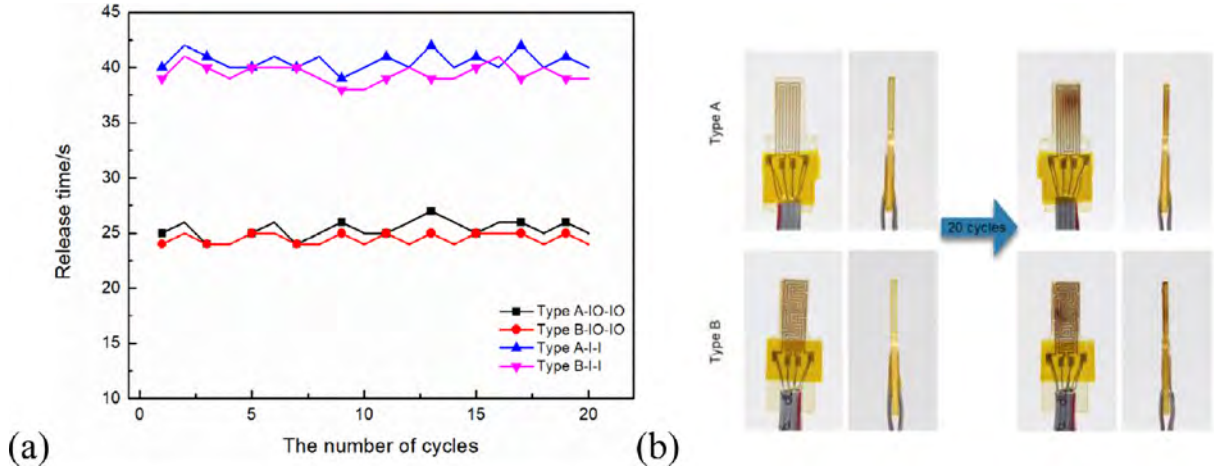

Fig. 17. Reusability of four types release devices under 3 V DC. (a) Curves of release time versus the number of cycles, (b) yellowed on ageing details.

5. Conclusions

An ultra-light release device integrated with screen-printed heaters has been designed and tested. Compared with existing HRMs for CubeSat's solar arrays, it has the advantage of structural integrity, improved heating reliability and good reusability. Firstly, static mechanical properties of spandex fiber reinforced SMPCs are obtained by tensile and fracture toughness tests. The results suggest that the 77.8dtex fibers show better toughness improvement performance than 141.4dtex fibers at the same fiber volume fraction. DMA tests reveal that the *Tg* of SMPC-77.8dtex has been decreased slightly compared with SMP. Locking forces obtained from both simulation and experiments show good consistency with acceptable errors. Besides, the temperature effect on locking properties has also been investigated by thermal cycles. Thereafter, vibration tests demonstrate that the CubeSat maintains a reliable packaged configuration without premature deployment nor fracture. Finally, shape memory recovery tests show good adaptability to energizing conditions and the release times of solar arrays are 25 s and 40 s for double-circuit and single-circuit heaters, respectively, 50% faster than free recovery. Furthermore, the 20 cycles of shape memory process show that the multi-use causes no significant deterioration in releasing response but some damages in morphology.

Acknowledgement

This work is supported by the National Natural Science Foundation of China (Grant No. 11632005 and 11672086).

References

[1] Peral E, Tanelli S, Statham S, Joshi S, Imken T, Price D, et al. RainCube: the first ever radar measurements from a CubeSat in space. J Appl Remote Sens 2019;13:032504.
[2] Chin A, Coelho R, Nugent R, Munakata R, Puigsuari J. CubeSat: the pico-satellite standard for research and education. Mol Syst Biol 2008;11:761–5.
[3] Li H, Liu X, Guo S, Cai G. Deployment dynamics and control of large-scale flexible solar array system with deployable mast. Adv Space Res 2016;58:1288–302.
[4] Li Y, Wang C, Huang W. Dynamics analysis of planar rigid-flexible coupling deployable solar array system with multiple revolute clearance joints. Mech Syst Signal Proc 2019;117:188–209.
[5] Purushothaman P. Launcher hold and release mechanism for GSLV. Proceedings of the 7th European Space Mechanisms and Tribology Symposium. 1997. p. 287.
[6] Abbas S, Jang J, Lee J, Kim Z. Development of an FPGA-based multipoint laser pyroshock measurement system for explosive bolts. Rev Sci Instrum 2016;87:073302.
[7] Thurn A, Huynh S, Koss S, Oppenheimer P, Butcher S, Schlater J, et al. A nichrome burn wire release mechanism for CubeSats. Proceedings of the 41st Aerospace Mechanisms Symposium. 2012. p. 479–88.
[8] Lee M, Lee Y, Kang S, Oh H. Launch and on-orbit environment verification test of flight model of hinge driving type holding and release mechanism based on the burn wire release. J Korean Soc Aeronaut Space Sci 2016;44:274–80.
[9] Tak W, Lee M, Kim B. Ultimate load and release time controllable non-explosive separation device using a shape memory alloy actuator. J Mech Sci Technol 2011;25:1141–7.
[10] Grulich M, Koop A, Ludewig P, Gutsmiedl J, Dietmann K. Smard-rexus-18: development and verification of an SMA based CubeSat solar panel deployment mechanism. Proceedings of the 22nd ESA Symposium European Rocket & Balloon Programmes and Related Research. 2015.
[11] Yoo Y, Jeong J, Lim J, Kim K, Hwang D, Lee J. Development of a non-explosive release actuator using shape memory alloy wire. Rev Sci Instrum 2013;84:015005.
[12] Khatsenko M. A rotary shape memory alloy actuator for CubeSat deployable structures Master's thesis Massachusetts Institute of Technology; 2017.
[13] Apland C, Persons D, Weir D, Marley M. A novel release mechanism employing the principle of differential coefficients of thermal expansion. Proceedings of the 41st Aerospace Mechanisms Symposium. 2012. p. 465–78.
[14] Baig H. Integrated design of solar panels deployment mechanism for a three unit CubeSat. Proceedings of the SpaceOps. 2012. p. 1–8.
[15] Leng J, Lan X, Liu Y, Du S. Shape-memory polymers and their composites: stimulus methods and applications. Prog Mater Sci 2011;56:1077–135.
[16] Mu T, Liu L, Lan X, Liu Y, Leng J. Shape memory polymers for composites. Compos Sci Technol 2018;160:169–98.
[17] Wang C, Wang Y. The mechanical design of a hybrid intelligent hinge with shape memory polymer and spring sheet. Compos B Eng 2018;134:1–8.
[18] Li F, Liu L, Lan X, Wang T, Li X, Chen F, et al. Modal analyses of deployable truss structures based on shape memory polymer composites. Int J Appl Mech 2016;8(07):1640009.
[19] An Y, Kim J, Goo N, Kim Y, Park J, Yu W. Quantitative evaluation of the three-dimensional deployment behavior of a shape memory polymer antenna. Smart Mater Struct 2018;27:105007.
[20] Liu T, Liu L, Yu M, Li Q, Zeng C, Lan X, et al. Integrative hinge based on shape memory polymer composites: material, design, properties and application. Compos Struct 2018;206:164–76.
[21] Lim J, Lee D, Kim H. Mechanical stretchability of screen-printed Ag nanoparticles electrodes on polyurethane substrate for stretchable interconnectors and thin film heaters. ECS J Solid State Sci 2018;7:468–72.
[22] Zeng P, Tian B, Tian Q, Yao W, Li M, Wang H, et al. Screen-printed, low-cost, and patterned flexible heater based on Ag fractal dendrites for human wearable application. Adv Mater Technol-Us 2019;4:1800453.
[23] Leng J, Wu X, Liu Y. Effect of a linear monomer on the thermomechanical properties of epoxy shape-memory polymer. Smart Mater Struct 2009;18:095031.
[24] Sun J, Liu Y, Leng J. Mechanical properties of shape memory polymer composites enhanced by elastic fibers and their application in variable stiffness morphing skins. J Intel Mat Syst Str 2015;26:2020–7.
[25] Chen J, Liu L, Liu Y, Leng J. Thermoviscoelastic shape memory behavior for epoxy-shape memory polymer. Smart Mater Struct 2014;23:055025.